These experiments show that the flow on the upper surface will follow a downward directed jet flap, even when the jet flap angle may be as much as 60°. The attached trailing edge flow on the upper (low pressure) surface is quite distinct from that on the lower (high pressure) surface. The jet flap diffuser fluid mechanics near the duct exit are *exactly* those of the low pressure trailing edge flow of a jet flap. Thus it is believed that the many successful jet flap experiments support the jet flap diffuser flow assumptions.

It is clear that entrainment will affect the performance of the jet flap diffuser. However, it is believed that this effect will be small. For the jet flap airfoil it is usual to assume that entrainment occurs with conservation of jet momentum, so that if the jet is thin (compared with the chord) the proper outer inviscid solution is that of a zero thickness jet of constant momentum. The theory developed by Spence[5] uses this assumption and has shown excellent correlation with experiment for a wide range of blowing coefficients and angles. Thus, it is believed that the inviscid analysis employed here is quite representative of the real viscous problem.

V. Summary and Conclusions

It appears that the jet flap diffuser will be a useful device for amplifying the thrust of an actuator, by effectively increasing its exit area. This may be of significance in cases where vehicle design precludes large mechanical diffusers, or where the propulsion system is capable of providing extra power.

Although the global and local analyses are done for the idealized case of the thin, inviscid jet it is believed that the results obtained do represent the dominant effects, and that the effective ranges of blowing coefficient and jet thickness indicated by this theory give the proper parameters for optimal design.

It is clear that experimental studies are the next important step, to assess the significance of turbulent entrainment on the performance of the jet flap diffuser.

References

[1] Luu, T.-S., "Contribution a la théorie linéarisée des effets de jets minces et de cavitations calcul des écoulements par analogie rhéoelectrique," thesis, Dec. 1960, Faculté des Sciences de l'Université de Paris.

[2] Morel, J.-P. and Lissaman, P. B. S., "The Jet Flap Diffuser: A New Thrust Augmenting Device," AIAA Paper 69-777, Los Angeles, Calif., 1969.

[3] Lazareff, M., "Hélices Carénées. Synthèse," TN ARA/NT/89/66, 1967, Nord-Aviation, France.

[4] Morel, J.-P. G., "Theoretical Solutions for the Jet Flap Diffuser," thesis, 1969, Dept. of Aeronautics, California Inst. of Technology, Pasadena, Calif.

[5] Spence, D. A., "The Lift Coefficient of a Thin Jet-flapped Wing," *Proceedings of the Royal Society of London*, Vol. 238, Jan. 1957, p. 46.

[6] Lissaman, P. B. S., "A Linear Theory for the Jet Flap in Ground Effect," *AIAA Journal*, Vol. 6, No. 7, July 1968, pp. 1356–1362.

[7] Lachmann, G. V., *Boundary Layer and Flow Control, Its Principles and Application*, Vol. 1, Pergamon Press, New York, 1961, pp. 343–364.

JULY 1971 J. AIRCRAFT VOL. 8, NO. 7

Studies of Engine-Airframe Integration on Hypersonic Aircraft

P. J. Johnston,* J. M. Cubbage,† and J. P. Weidner‡
NASA Langley Research Center, Hampton, Va.

Effects of turbo-ramjet exhaust impingement on performance, stability, and control of a Mach 6 transport, and thrust vectoring on a scramjet powered Mach 12 vehicle were investigated. Simplified theories for predicting performance benefits from exhaust interference were in agreement with experimental results for the transport. Scramjet engine integration on a Mach 12 lifting body configuration was studied parametrically, and the effects of engine location, thrust deflection, and altitude were evaluated on the basis of cruise Breguet factor. Losses due to trim penalties could be minimized by careful consideration of engine integration as well as vehicle static margin.

Nomenclature

A_c = inlet capture area
BF = Breguet factor, $V(L/D)I_{sp}$, naut miles
C_p = pressure coefficient $p_l - p_\infty/q_\infty$
D = drag, lb
d_e = nozzle exit diam, ft
F_g = gross thrust, lb
F_N = net thrust, lb
h = altitude, ft
I_{sp} = installed specific impulse, Drag/$\dot{w}_F$, sec
l = pitching-moment reference length (equal body length for lifting body, mean aerodynamic chord for airplane model)
L = lift, lb
M = Mach number
m = moment, ft-lb
p = static pressure, lb/ft^2
q = dynamic pressure, lb/ft^2
R_l = Reynolds number
S = reference area, ft^2
V = velocity, fps
$\dot{w}_F$ = fuel flow, lb/sec
x = longitudinal distance, ft
α = angle of attack, deg
γ = specific heat ratio
θ_{F_g} = thrust vector angle, positive when exhaust is deflected downward from body axis
δ_e = elevon deflection angle, positive trailing edge down

Presented as Paper 70-542 at the AIAA Atmospheric Flight Mechanics Conference, Tullahoma, Tenn., May 13–15, 1970; submitted June 6, 1970; revision received October 21, 1970.

* Aerospace Engineer, Hypersonic Aircraft Systems Research Branch, Hypersonic Vehicles Division. Member AIAA.

† Aerospace Engineer, Hypersonic Aircraft Systems Research Branch, Hypersonic Vehicles Division.

‡ Aerospace Engineer, Hypersonic Propulsion Branch, Hypersonic Vehicles Division.

Subscripts

c = cowl
e = exhaust or engine
i = inlet
j = jet on
0 = without engine package installed
l = local
max = maximum
∞ = freestream
1 = average conditions in wing flowfield

Introduction

ENGINE-airframe integration has been an important problem in the design of many transonic and supersonic aircraft; however, as the speed increases into the hypersonic range, the problem takes on entirely new dimensions. Not only does the relative size of the engine (as measured by the freestream capture area) increase by an order of magnitude as the Mach number increases from 2 to 12, but also the engine forces increase rapidly. The net thrust is the difference between two large and nearly equal forces—the nozzle thrust and the ram drag. At a Mach number of 12, for example, the gross nozzle thrust can be an order of magnitude greater than the net thrust required to propel the airplane.

Previous work[1,2] has shown that deflection of the large gross thrust vector can yield significant gains in lift with little loss in available thrust. In addition, Ref. 3 showed that high, the pressures of an underexpanded nozzle flow of a Mach 6 transport configuration could provide favorable interference effects if the exhaust flow washed a large area of the wing lower surface. In general, however, these studies neglected many of the other interactions between the engine and airframe such as trimming the aircraft in the presence of large engine forces.

It is the purpose of this paper to explore analytically and experimentally some of the consequences of the interaction of these large forces on the airframe-propulsion system integration for a Mach 6 hypersonic transport concept, and for a Mach number 12 hypersonic research airplane concept.

Results and Discussion

Jet Interference Effects on the Aerodynamics of a Mach 6 Cruise Aircraft

Turbo-ramjet engines, consisting of turbo-accelerators for Mach numbers up to 3 and subsonic burning ramjets for higher speeds, have been proposed as propulsion systems for Mach 6 aircraft. The analysis of Ref. 3 showed that, at cruise, the nozzle flow for these engines will be underexpanded because of a compromise between maximum propulsion efficiency and engine nacelle drag. Figure 1 shows nozzle static pressure ratios as a function of nacelle expansion ratio for typical ramjet component efficiencies. Since no effects from the airframe are included other than the strength of the wing shock, the data are represented by a band covering the angle-of-attack range from 0° to 8°. Also shown are the nozzle static pressure ratios obtained for in-line or wrap-around turbo-ramjet engines on the blended wing-body Mach 6 cruise aircraft of Ref. 4. These pressure ratios were determined by a mission analysis computer program which sizes the engines for a particular set of aircraft aerodynamics. The nacelle exit area, A_e, for these engines was restricted to the maximum engine diameter because larger exit areas resulted in large drag increments. The pressure ratios of 2.5 for the in-line and 1.8 for the wrap-around turbo-ramjets are used as reference conditions in the following discussion.

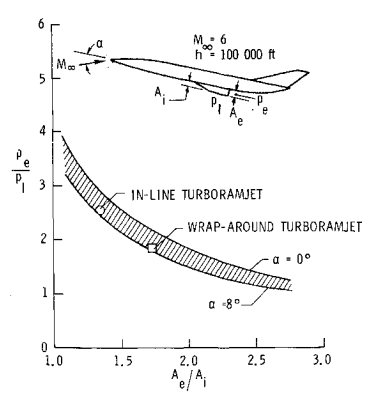

Fig. 1 Typical nozzle-exit static pressure ratios.

Flowfield characteristics

To provide a better understanding of nozzle exhaust flow effects, experimental data were obtained at a Mach number of 6 on a flat-plate model with four adjacent axisymmetric nozzles as shown in Fig. 2. The inlet flow was discharged rearward from the lee surface to prevent interference with the nozzle exhaust flow. High-pressure air was used as the working fluid in the M_e = 3.5 nozzles. The pressure distribution downstream of the nozzles shown in Fig. 2 is typical for other pressure ratios and angles of attack. At the nozzle exits, maximum pressures occur on the nozzle center lines, and minimum pressures occur between the nozzles (because of aspiration by the nozzle flow). Downstream of the exit plane, the nozzle flows impinge on each other causing a high-pressure region to occur between adjacent nozzles while along the nozzle center lines, the expansion of the exhaust flow causes the pressure to decrease in the axial direction. The high pressures between the nozzles decay to isolated flat-plate pressures 2 to 6 nozzle diameters downstream of the exit plane (depending on nozzle pressure ratio), because the expansion waves from the lower portion of the nozzle lip impinge on the plate surface.

Effect of nozzle flow on the performance and stability of a Mach 6 cruise aircraft

Representative forces induced by nozzle flow were also obtained experimentally on a model of the hypersonic cruise transport of Ref. 5. Since it was not essential for these tests, the vertical tail was removed, as indicated by the sketch on the left of Fig. 3. Pressure orifices were limited to the wing lower surface, as shown, to minimize the interference effects from the support strut. A mixture of sulfur hexafluoride (75% by weight) and nitrogen (25% by weight) was used for simulation of the nozzle exhaust flow. This gas mixture, at a total temperature of 350°F, yielded a ratio of specific heats at the nozzle exit of 1.26 which is considered to be typical of a hydrogen-fueled turbo-ramjet. The exit Mach number of the nozzles was 3.7. Air approaching the simulated propulsion nacelle was captured by an inlet and discharged rearward from an opening in the top of the model.

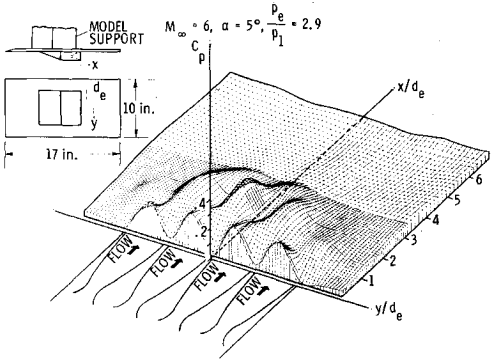

Fig. 2 Surface pressure coefficients downstream of nozzle exits.

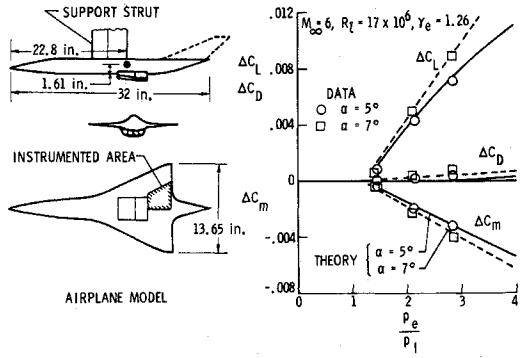

Fig. 3 Test model and incremental force and moment data due to jet interference.

Incremental lift, drag, and pitching-moment coefficients resulting from jet interference effects are shown in Fig. 3 for two angles of attack which bracket $(L/D)_{max}$. These increments represent the differences between the integrated pressure distributions with nozzle flow and those obtained with the propulsion system nacelle removed. The experimental coefficients have a nearly linear variation with nozzle static pressure ratio and the theory, described in Ref. 6, is in good agreement with the experiment because the analysis accounted for the average momentum imparted to the exhaust flow. Note that if the data are extrapolated to pressure ratios below about 1.25, a lift decrement occurs because of the aspirating effect of the jets at low static pressure ratios. (Results obtained on the flat-plate model confirmed the validity of this extrapolation.)

Figure 4 shows the lift-drag ratio in the presence of the jet interference normalized by the lift-drag ratio of the model with a flow-through inlet installed (obtained from Ref. 5). Maximum experimental L/D increments were about 6% for typical pressure ratios of an in-line turbo-ramjet, and about half that value for the wrap-around turbo-ramjet. Performance decrements occur at pressure ratios below about 1.25 because of the loss in lift due to aspiration noted above.

The effects of jet interference on pitching moment are illustrated in Fig. 5. The airplane-alone moment data shown here were obtained on the flow-through inlet model of Ref. 5. At a nozzle static pressure ratio of 2.0, the effects of displacing the net thrust below the center of gravity are counteracted by the negative increments due to jet interference so that no additional aerodynamic control deflections would be required to trim out moments due to the propulsion system. At lower angles of attack, the pressure ratio for mutual cancellation of the opposing moments decreased to a value of 1.5 at $\alpha = 0°$. As shown on the right of Fig. 5, the propulsion system forces had negligible effects on the stability at angles of attack near $(L/D)_{max}$ ($5° \leq \alpha \leq 7°$) for the range of pressure ratios of interest.

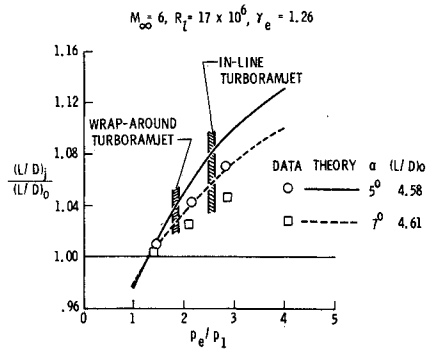

Fig. 4 Jet effect on airplane performance.

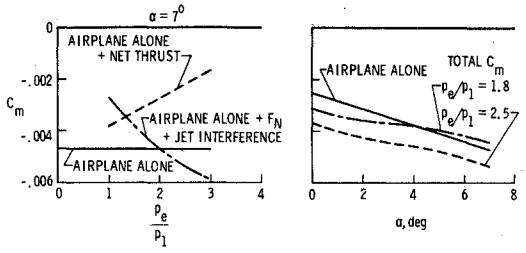

Fig. 5 Propulsion system effects on pitching moment.

Comparison of the effect of jet interference and thrust vectoring

Thrust vectoring or deflection to improve cruise range has been shown[7] to be particularly applicable to hypersonic aircraft because the gross thrust (the quantity vectored) of an air-breathing propulsion system is much larger than the net thrust of the system at hypersonic speeds. Therefore, it is of interest to compare the Breguet factor of an aircraft subject to jet interference effects with that obtainable for the same aircraft using thrust vectoring. In calculating the Breguet factor for either case, estimates of the variation of L/D, F_N/F_g, and specific impulse with A_e/A_i were made and are shown in Fig. 6. These parameters are typical of a Mach 6 turbo-ramjet powered hypersonic transport during the cruise phase of the flight at an angle of attack of 5°. The variation of nozzle pressure ratio with A_e/A_i presented in Fig. 1 was used along with the incremental force data due to jet interference obtained from experimental results on the flat plate.

Figure 7 shows that thrust vectoring and jet interference are equally effective in improving the Breguet factor. The curve for no-jet interference or thrust vectoring reflects only the changes in airframe and engine performance parameters with expansion ratio shown in the previous figure, and is representative of a configuration with the nozzle exit plane coincident with the wing trailing edge.

Jet interference has a detrimental effect on Breguet factor at values of A_e/A_i greater than 2 because of the lift decrement noted previously for nozzle pressure ratios of about 1.25 or less. Although the efficiency of the nozzles is decreasing at low values of A_e/A_i, jet interference is more effective than thrust vectoring because the wing lower surface acts as a nozzle, both expanding the exhaust flow and deflecting it downward achieving the dual effect of effectively increasing the nacelle expansion ratio and vectoring the thrust with no decrease in L/D.

At area ratios above about 1.7, the Breguet factor for the vectored thrust case begins to decrease because of a rapid loss in L/D due to nacelle drag. If full expansion of the nozzle flow could be achieved without incurring this drag penalty (for example, by allowing the nozzle contour to penetrate the body and sacrificing volume for nozzle expansion area) a maximum Breguet factor of 16,450 naut miles could be achieved by vectoring the thrust to the optimum deflection angle.

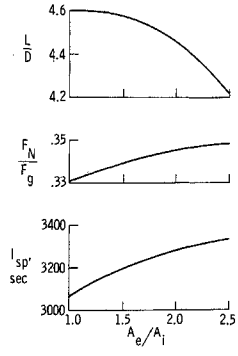

Fig. 6 Variation of parameters used in Breguet factor calculation with nacelle expansion ratio.

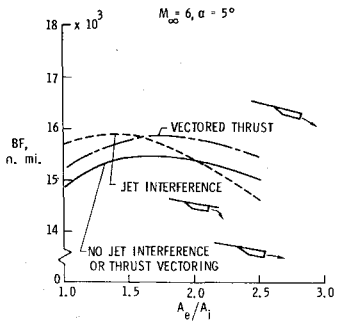

Fig. 7 Effect of jet interference and thrust vectoring on Breguet factor.

These studies at $M = 6$ have shown that the over-all effect of jet interference on aircraft performance was beneficial, and that it could be as effective as thrust vectoring in improving the cruise Breguet factor. For the engine size and placement considered, the pitching moment due to jet interference essentially canceled the moment produced by the engine net thrust so that performance penalties, in the form of additional trim drag increments, were not incurred as a result of integrating the engine and airframe.

Scramjet Integration Studies

In contrast to the situation at Mach 6, where the displacement of the bow shock is large enough to permit some latitude in engine placement and design, the shock at Mach 12 is much closer to the body. Therefore, for a given body location, the inlet vertical dimension will be limited to the height of the shock layer. In addition, for satisfactory engine performance, it is essential that the exhaust nozzle have a large expansion ratio. Thus, a distinguishing feature of the integration of the engine and airframe at high Mach numbers is the use of large fractions of the afterbody as part of the engine exhaust nozzle.

Vehicle description

In order to determine the consequence of the foregoing characteristics on the performance and longitudinal stability of a Mach 12 vehicle, an analysis was made on the configuration shown in Fig. 8. The shape evolved from NASA Langley studies of a research airplane which could be employed as a test bed for air-breathing propulsion research. It was rocket boosted so that the maximum operating envelope would not be limited by the research engine performance. Except for this aspect of boost propulsion, the vehicle conforms in many ways to concepts recently developed as hypersonic cruise and air-breathing launch aircraft. The vehicle is trimmed in pitch by all movable elevons hinged at their $\frac{2}{3}$ chord point, and situated outboard of the vertical tails.

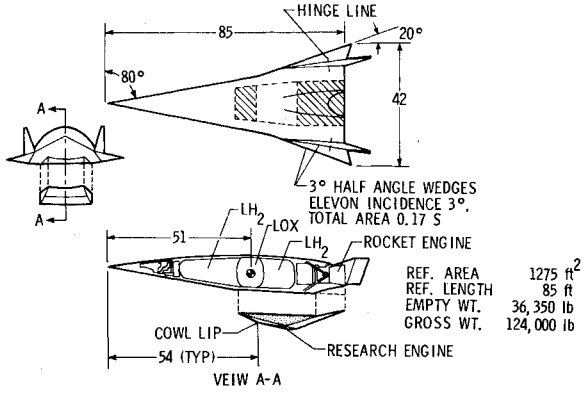

Fig. 8 Mach 12 research airplane.

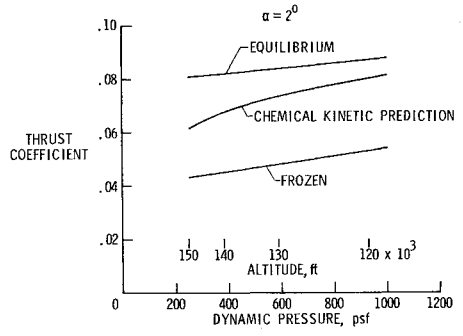

Fig. 9 Effect of chemical kinetics on engine performance.

Propulsion system concepts

The research engine studied is a hydrogen-fueled, supersonic-combustion ramjet, which was assumed to operate over the Mach number range from 6 to 12. In order to facilitate the analysis, the engine was chosen to be of a two-dimensional, rather than a three-dimensional design although the latter might offer significant improvements in areas such as inlet starting capability, cooling requirements, and so forth. The engine was designed with relatively weak internal shocks, and had a contraction ratio of 9 between a station on the forebody at the beginning of the ramp and the combustor, which yielded an over-all contraction ratio of 25 to 35 depending on angle of attack. The inlet was designed to operate shock-on-lip at $M \approx 12$, and the vertical and streamwise dimensions of the engine were scaled in proportion to the height of the shock layer at the position of the inlet on the body.

The gross thrust vector orientation was changed by varying the initial nozzle expansion angle. The exhaust nozzle contour was always chosen to be on-design at a velocity of 12,000 fps with all expansion waves canceled at the wall. This design provided uniform flow across the last expansion wave emanating from the cowl trailing edge and intersecting the nozzle wall at the vehicle base.

In the planform view, the sides of the engine ahead of the combustor were assumed to lie along rays originating at the vehicle nose. Sidewalls were assumed to extend from the cowl lip to the intersection of the compression ramp and forebody to prevent lateral spillage. Similarly, streamwise sidewalls were provided downstream of the combustor to insure two-dimensional flow and the elimination of lateral expansion in the nozzle. The fuel was assumed to be burned stoichiometrically at the design velocity.

At the altitudes of interest in this study, chemical kinetics in the nozzle flow can have a marked effect on engine performance. To account for these effects, a finite-rate chemical kinetics computer program was used to predict the deviation of nozzle thrust away from chemical equilibrium. Typical results are given in Fig. 9 which shows the predicted

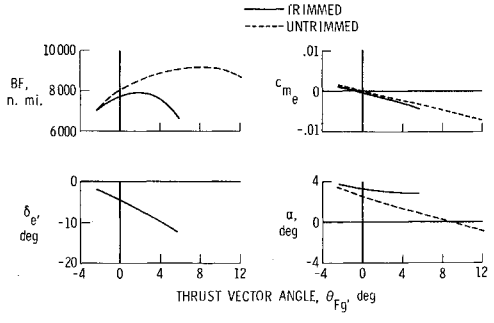

Fig. 10 Effect of thrust vectoring on Breguet factor and stability.

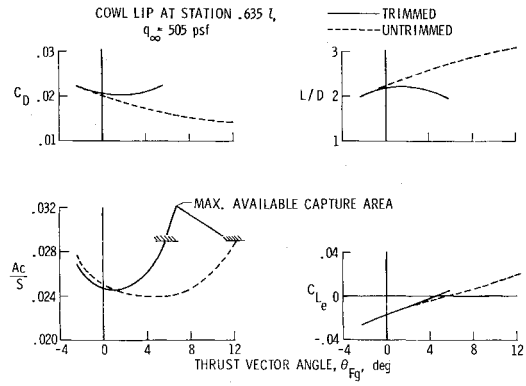

Fig. 11 Effect of thrust vectoring on engine size and vehicle performance.

thrust coefficients relative to the equilibrium and frozen values for a representative angle of attack.

Analytical procedures

The vehicle external aerodynamic forces were determined by use of the Hypersonic Arbitrary Body Computer Program of Ref. 8. Tangent-cone theory was used on windward surfaces of the body and cowl exterior. Leeward surface pressures were obtained by isentropic expansion of free-stream flow to the local surface slope. Shock-expansion theory was applied over the elevons and vertical tails. Fully turbulent boundary-layer conditions were assumed, and the skin friction calculated at $\alpha = 0°$ was assumed constant with angle of attack.

Engine and airframe force allocation

In accounting for the aerodynamic and propulsive forces, it was assumed that the engine began at the juncture of the compression ramp and the forebody, and the forces on the ramp as well as the exposed nozzles were accounted for in computing the engine performance (see shaded areas in Fig. 8). Except for these two areas, the aerodynamic forces on all other surfaces were charged to the airframe. The final integrated vehicle characteristics were obtained by summing the airframe aerodynamic and net engine force and moment contributions. The engine size was determined uniquely by matching the wind axis net thrust component and the trimmed or untrimmed drag. In addition, the specific impulse is an installed value, defined as the ratio of drag to fuel flow rather than the customary ratio of net thrust to fuel flow obtained from the usual one-dimensional engine cycle calculations.

Effects of thrust vectoring on longitudinal characteristics

Figures 10–12 illustrate the typical effect of varying the gross thrust vector angle on the longitudinal stability and

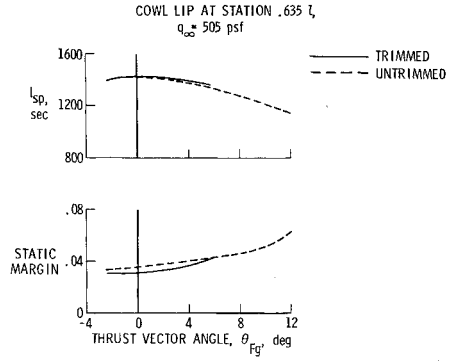

Fig. 12 Effect of thrust vectoring on I_{sp} and static margin.

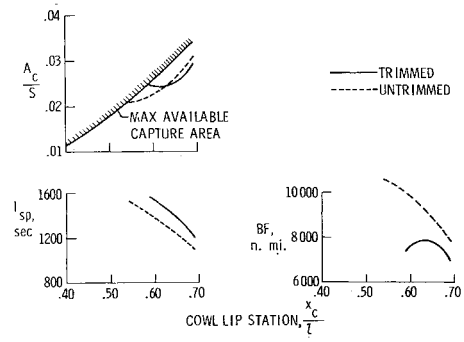

Fig. 13 Effect of engine location on size and performance.

performance characteristics at a velocity of 12,000 fps. These data were obtained at a constant total lift coefficient (including aerodynamic and propulsive lifts) of 0.044 and correspond to a dynamic pressure of 505 psf or an altitude of 133,500 ft.

Increasing the gross thrust vector angle (Fig. 10) provided improvements in both the untrimmed and trimmed Breguet factor, but trimming the aircraft resulted in an appreciable reduction in the maximum value. An insight into the factors contributing to this loss in performance can be gained by an examination of the parameters shown in Figs. 10–12. Consider first the engine pitching-moment contribution, which, as shown in Fig. 10, becomes more negative as the gross thrust vector angle is increased. Large negative elevon deflections are required to trim out the moment contributions at large values of θ_{F_g}. To overcome the negative lift of the elevons and maintain a constant altitude or total lift coefficient, the angle of attack must be increased relative to the untrimmed case, hence, additional drag increments are incurred due to trim (see Fig. 11). As a result of this additional drag, the engine size for the trimmed vehicle increases much more rapidly with θ_{F_g} than for the untrimmed case.

The installed specific impulse or the ratio of drag to fuel flow decreases somewhat with θ_{F_g}, as shown in Fig. 12, because smaller components of the net thrust are available to overcome the drag when the engine exhaust deflection is increased. When related to the improvements in untrimmed Breguet factor, however, these decrements in I_{sp} are small, percentagewise, compared to the large benefits in lift-drag ratio produced by thrust vectoring.

Figure 12 also indicates the static margin increases with gross thrust vector angle for both the trimmed and untrimmed vehicles.

Effect of engine translation on performance

As a first attempt in alleviating the range penalties due to trim, the engine longitudinal position on the airframe was varied. In addition to its effects on the engine pitching-

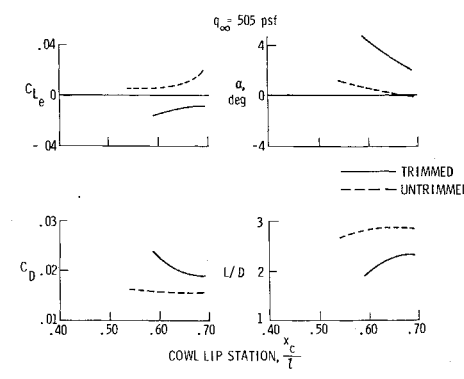

Fig. 14 Effect of engine location on performance.

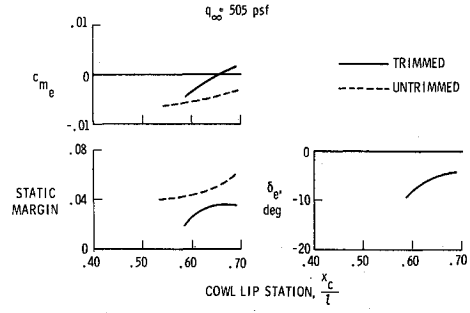

Fig. 15 Effect of engine location on stability and control.

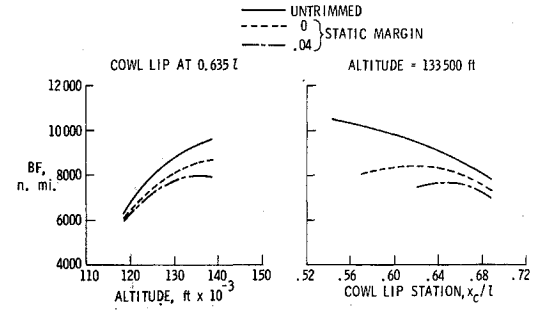

Fig. 17 Effects of static margin on performance.

moment contribution, translation of the engine also affected specific impulse because this parameter is sensitive to the nozzle expansion ratio. Translation actually had two effects on the expansion ratio: first, it increased as the engine was moved forward because the nozzle became longer. Second, the engine vertical dimensions were scaled according to the shock-layer height; consequently, as the engine was moved toward the nose, the height of the combustor became smaller, and provided an additional favorable increase in nozzle expansion ratio.

Figures 13–15 summarize the effects of longitudinal engine position on aircraft stability and performance. These data are limited to engine-airframe combinations providing either maximum trimmed or untrimmed Breguet factors at a given body station.

As indicated in Fig. 13, there is a longitudinal position on the vehicle that yields a minimum-capture-area engine for the trimmed aircraft. The boundary curve represents the longitudinal variation of maximum capture area, as determined by the product of the local span and the shock-layer height. The improvements in specific impulse stemming from a forward translation of the engine are evident in Fig. 13. Values of I_{sp} for the trimmed aircraft are higher than for the untrimmed vehicle because optimum trimmed Breguet factors occur at thrust vector angles which are smaller than for the untrimmed case, and installed specific impulse tends to decrease with θ_{F_g} (see Fig. 12).

According to Fig. 13, the Breguet factor for the untrimmed aircraft increases as the engine is moved toward the nose. These increases are related primarily to the improved I_{sp} rather than to variations in L/D which, as shown in Fig. 14, do not exhibit significant changes with cowl location.

Figure 13 also indicates that the differences between the trimmed and untrimmed Breguet factors increase as the engine is moved forward, and result from the greater trim drag penalties associated with these engine locations. (See Fig. 14). The source of these higher trim drags is shown in Figs. 14 and 15. For example, the engine lift and moment contributions become more negative as the engine is moved forward, requiring both higher angles of attack and more negative elevon deflections to achieve trim at a constant lift coefficient.

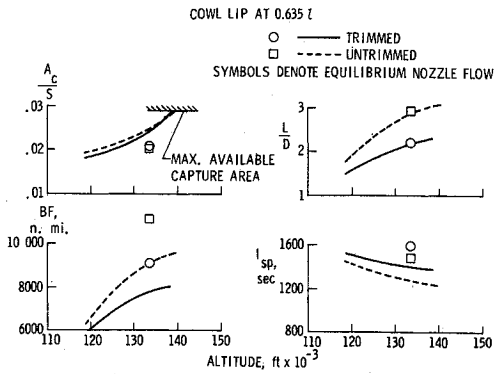

Fig. 16 Altitude effects on vehicle performance.

As shown in Fig. 15, the aircraft static margin tends to decrease as the engine is moved forward on the body with the trimmed vehicle exhibiting the lower stability level.

Altitude effects on vehicle performance

The previous results illustrating the effect of thrust vectoring and engine location on vehicle characteristics were obtained at a fixed altitude which did not correspond to that for maximum Breguet factor. To determine the best cruise altitude, it is necessary to evaluate the integrated vehicle performance at several altitudes because of the opposing effect altitude has on vehicle aerodynamics and engine performance. For example, scramjet engine performance deteriorates with altitude primarily because of adverse real-gas effects. On the other hand, the airframe may compensate for this unfavorable effect by operating closer to $(L/D)_{max}$.

To examine the effect of altitude on cruise performance, an engine location was selected with the cowl lip at $0.635l$ since the previous data showed this position yielded the highest trimmed Breguet factor at a dynamic pressure of 505 psf. Engine performance was degraded with altitude by accounting for the deviation of the combustion process away from equilibrium flow as indicated previously in Fig. 9.

The effect of altitude on the major vehicle performance parameters is shown in Fig. 16. As expected, altitude had an adverse effect on installed specific impulse, however, the vehicle aerodynamic performance more than compensated for this reduction with the result that the cruise Breguet factors increase over the altitude range. It is also apparent that the maximum engine capture area was reached at a lower altitude than that required for best cruise Breguet factors. A low wing loading aggravated by large centrifugal relief effects due to the high cruise velocity was the primary reason for this situation.

The losses in Breguet factor and L/D due to trim penalties increased with altitude, however, the effects of trim on engine capture area were generally small.

In order to illustrate the effect nonequilibrium chemistry can have on scramjet cruise performance at high Mach numbers, additional calculations were made at an altitude of 133,500 ft assuming the exhaust flow was either in equilibrium or remained entirely frozen. Typically, the engine performance was so poor under the latter assumption that the inlet areas exceeded the maximum available capture area ratios by more than 25%. The assumption of chemical equilibrium in the exhaust resulted in about a 17% increase in trimmed Breguet factor and in a reduction in engine capture area ratio of about the same magnitude.

Effect of static margin on performance

The foregoing results were for a center of gravity of $0.604l$ which was arrived at by preliminary weight and balance studies. On this basis, engine-airframe combinations exhibiting a maximum trimmed Breguet factor have varying stability levels depending on the engine location on the body (Fig. 15). In Fig. 17, the previous data are compared on the

basis of constant static margins of zero (neutrally stable) and 4% of the fuselage length. The results on the left of Fig. 17 show that the range losses due to trim increased with altitude (C_L), and that nearly half of the performance decrements due to trim could be recovered by reducing the static margin to zero. As shown on the right of Fig. 17, the optimum engine location tends to move forward as the static margin is reduced. A 4% reduction in static margin improved the maximum trimmed Breguet factor by 10% at an altitude of 133,500 ft, and additional benefits can be expected at higher altitudes.

In addition to the foregoing studies, a brief investigation of flight at off-design conditions indicated that stability and control did not appear to be a major problem area for this configuration.

Concluding Remarks

Important gains in hypersonic aircraft performance can be derived from thrust vectoring and exhaust interference, however, the trim forces required to overcome possible engine pitching moments must be included in the optimization of the engine-airframe integration. When the engine and the area over which the exhaust flow acts can be located near the aircraft center of gravity, as was the case with the Mach 6 transport configuration, trim effects were small and full integration benefits can be achieved. On the other hand, when nearly the entire lifting surface of the airplane is part of the engine, as in the case of highly integrated configurations, large engine moments can exist and full advantage of thrust vectoring may not be realized because of large trim forces. For the Mach 12 aircraft considered here, these trim forces resulted in performance losses on the order of 10% for the optimum engine-airframe combination. The degree to which these losses are dependent on aircraft geometry is, of course, unknown and warrants additional study.

Experimental results obtained at $M = 6$ on the transport configuration showed that the lower surface of the wing aft of the engine nozzle exit could be used to expand the exhaust flow and provide a form of thrust vectoring. Although the flow was extremely complex, it was shown that the over-all effects could be adequately predicted by a simplified theoretical analysis.

References

[1] Williams, L. J. and Wilcox, D. E., *Scramjet Vehicle Engine-Airframe Integration Effects*, (Conference on Hypersonic Aircraft Technology, NASA Ames Research Center, Moffett Field, Calif.,) NASA SP-148, May 1967.

[2] Gregory, T. J., Wilcox, D. E., and Williams, L. J., "The Effects of Propulsion System-Airframe Interactions on the Performance of Hypersonic Aircraft," AIAA Paper 67-493, Washington, D.C., 1967.

[3] Kirkham, F. S., Cubbage, J. M., Vahl, W. A., and Small, W. J., "Studies of Airframe-Propulsion System Integration for Mach 6 Cruise Vehicles," TN D-4128, 1967, NASA.

[4] Jarlett, F. E., "Performance Potential Hydrogen Fueled, Airbreathing Cruise Aircraft," Rept. GDC-DCB-66-004/1–66-004/4, NAS 2-3180, May and Sept. 1966, General Dynamics/Convair Division, San Diego, Calif.

[5] Penland, J. A., Edwards, C. L. W., Witcofski, R. D., and Marcum, D. C., *Comparative Aerodynamic Study of Two Hypersonic Cruise Aircraft Configurations Derived From Trade-Off Studies*, (Conference on Hypersonic Aircraft Technology, NASA Ames Research Center, Moffett Field, Calif.,) NASA SP-148, 1967.

[6] Cubbage, J. M. and Kirkham, F. S., "Investigation of Engine-Exhaust-Airframe Interference on a Cruise Vehicle at Mach 6," TN D-6060, 1970, NASA.

[7] Krase, W. H., "Thrust Deflection for Cruise," *Journal of Aircraft*, Vol. 4, No. 2, March-April 1967, pp. 162–163.

[8] Gentry, A. E., "Hypersonic Arbitrary-Body Aerodynamic Computer Program, Mark III Version," *User's Manual*, Vol. I, Rept. DAC61552, April 1968, Douglas Aircraft Co., McDonnell Douglas Corp., Long Beach, Calif.